

Experimental test of the universal differential fluctuation theorem with a levitated nanosphere

Thai M. Hoang,^{1,*} Rui Pan,² Jonghoon Ahn,³ Jaehoon

Bang,³ H. T. Quan,^{2,4,†} and Tongcang Li^{1,3,5,6,‡}

¹*Department of Physics and Astronomy,*

Purdue University, West Lafayette, IN 47907, USA

²*School of Physics, Peking University, Beijing 100871, China*

³*School of Electrical and Computer Engineering,*

Purdue University, West Lafayette, IN 47907, USA

⁴*Collaborative Innovation Center of Quantum Matter, Beijing 100871, China*

⁵*Purdue Quantum Center, Purdue University, West Lafayette, IN 47907, USA*

⁶*Birck Nanotechnology Center, Purdue University, West Lafayette, IN 47907, USA*

(Dated: December 14, 2024)

Abstract

Nonequilibrium processes of small systems such as molecular machines are ubiquitous in biology, chemistry and physics, but are often challenging to comprehend. In the past two decades, several exact thermodynamic relations of nonequilibrium processes, collectively known as fluctuation theorems, have been discovered and provided critical insights. These fluctuation theorems are generalizations of the second law, and can be unified by a universal differential fluctuation theorem. Here we perform the first experimental test of the differential fluctuation theorem, using an optically levitated nanosphere in both underdamped and overdamped regimes, and in both spatial and velocity spaces. We also test several theorems that can be obtained from it directly, including the Jarzynski equality, the Crooks fluctuation theorem, the Hummer-Szabo relation, and a generalized Jarzynski equality that is valid for arbitrary initial states. Our study experimentally verifies these theorems and advances our understanding of nonequilibrium thermodynamics.

* Current address: Sandia National Laboratories, Albuquerque, NM 87123

† Corresponding author: htquan@pku.edu.cn

‡ Corresponding author: tcli@purdue.edu

In the past two decades, there were significant developments in nonequilibrium statistical mechanics of small systems in which thermal fluctuation is influential [1]. The most prominent progresses are the discoveries of various fluctuation theorems (FT), which connect microscopic dynamics with thermodynamic behaviors [1]. These FT, such as the Jarzynski equality (JE) [2, 3] and the Crooks fluctuation theorem (CFT) [4, 5], reformulate the inequality of the second law into equalities, and reveal the universal laws that the fluctuating thermodynamic variables must obey in processes arbitrarily far from thermal equilibrium. As they are refinements of the second law on individual trajectories, they provide critical understandings of behaviors of biological systems at the single molecular level [3, 5–10] and nonequilibrium dynamics of a wide range of physical systems [11–26].

In 2008, a universal differential fluctuation theorem (DFT) connecting the joint probabilities of work/heat and arbitrary generalized coordinates (e.g. position and velocity coordinates) was derived by Maragakis, Spichty and Karplus [20]. It is remarkable that the DFT can unify various FT as long as detailed balance is not violated [20]. Such ability is rooted from the fact that most FT originate from the same fundamental principle: the microscopic reversibility connecting forward and reverse trajectories [1, 18, 24, 27–29]. Testing the DFT would provide a detailed fundamental understanding of the second law and nonequilibrium physics, including irreversibility, dissipation and hysteresis. In order to test the DFT at its desired level of detail, we need large statistics and the ability to track individual trajectories of a stochastic process in the phase space [20], which requires the measurement of instantaneous velocities of Brownian motion [30].

In this work, we experimentally test the differential fluctuation theorem [20] using an optically levitated nanosphere which can be trapped in air continuously for weeks for acquiring large sets of data. Our ultrasensitive optical tweezer can measure both instantaneous position and instantaneous velocity [30] of a levitated nanosphere to test DFT. Over one million experimental cycles per setting ($\sim 10^{10}$ position data points per setting) provide sufficient statistics to validate the DFT at its desired level of detail, e.g., testing DFT for nonequilibrium processes connecting two points in the position-velocity space [20]. Several fluctuation theorems, including the Jarzynski equality [2, 3], the Crooks fluctuation theorem [4, 5], the Hummer-Szabo relation (HSR) [6–8], a generalized JE [19, 24, 27], the extended fluctuation relation (EFR) [9, 10], and the fluctuation theorem for ligand binding (FTLB) [31] can be unified by the DFT [18, 24, 27, 28]. We have also tested several such theorems. In our ex-

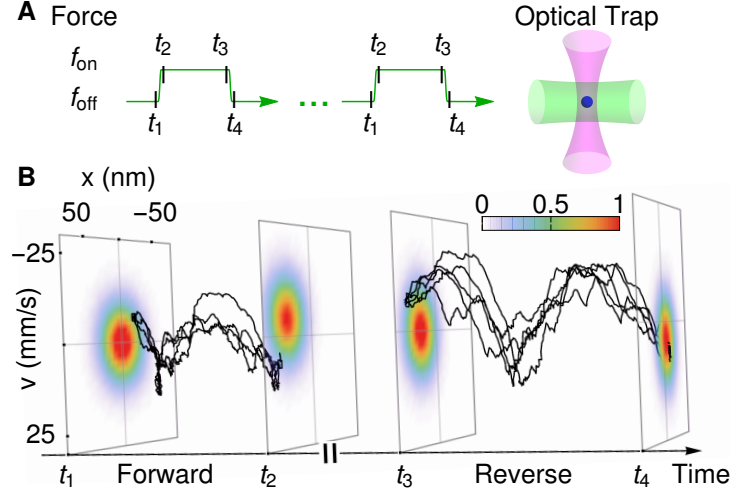


FIG. 1. **A**, Experimental scheme. A silica nanosphere (blue sphere) is trapped in an optical tweezer formed by a focused 1550-nm laser beam (magenta). A series of 532-nm laser pulses (green) exerts an optical force on the nanosphere to drive nonequilibrium processes. Within each pulse, an optical force is rapidly ramped from f_{off} at time t_1 to f_{on} at time t_2 during the forward process (green pulse). The reverse process from time t_3 to t_4 is the time-reversed correspondence of the forward process. **B**, An example of experimental data. Vertical slides represent the measured time snapshots of the probability distributions at times t_1 , t_2 , t_3 , and t_4 as illustrated in **A**. Black curves represent experimental phase-space trajectories during forward processes initialized at (x_1, v_1) and finalized at (x_2, v_2) , and during reverse processes initialized at the $(x_2, -v_2)$ and finalized at $(x_1, -v_1)$. Here $x_1 = -19$ nm, $x_2 = 55$ nm, $v_1 = -7$ mm/s, and $v_2 = 7$ mm/s. The nanosphere is levitated in air at 50 torr, and $f_{\text{off}} = 0$, $f_{\text{on}} = 340$ fN.

periment, the air pressure can be adjusted to test these theorems in both underdamped and overdamped regimes. This study demonstrates a powerful approach applicable in exploring a wide range of nonequilibrium systems [3, 5–13, 15, 16] since a complete description of the stochastic system includes the information of both position and velocity.

Our experiments are carried out using a silica nanosphere levitated by a 1550 nm optical tweezer (Fig. 1A) [32]. The nonequilibrium processes are controlled by a force parameter f which is an optical force exerted on the nanosphere by a 532-nm laser beam. In a forward process, the optical force is ramped from f_{off} at time t_1 to f_{on} at time t_2 . The reverse process

is from t_3 to t_4 . The DFT connects the forward and reverse processes as [20, 29]:

$$P_R(-W, b^* \rightarrow a^*) / P_F(W, a \rightarrow b) = e^{-\beta(W - \Delta F)}, \quad (1)$$

where a , b can be arbitrary generalized coordinates. In our work, the forward or reverse process starts from an equilibrium state by holding the optical force constant before the ramps. a and b denote the position (x) and/or velocity (v) coordinate, e.g., a can be x , or v , or (x, v) . $P_F(W, a \rightarrow b)$ is the forward joint probability of performing nonequilibrium work W for those trajectories starting from a and ending at b , and $P_R(-W, b^* \rightarrow a^*)$ is the reverse joint probability. The work distribution $P_F(W)$ can be obtained by integrating $P_F(W, a \rightarrow b)$ over a and b . The asterisk (*) denotes a reversal of the velocity components of a or b . $\Delta F \propto (f_{\text{off}}^2 - f_{\text{on}}^2)$ is the free energy difference between the equilibrium states of the optical forces f_{on} and f_{off} . $\beta = 1/(k_B T)$, where k_B is the Boltzmann constant, and $T = 296$ K is the room temperature.

To test the DFT in detail, over one million experimental forward-reverse cycles (500 $\mu\text{s}/\text{cycle}$) are performed for a given irreversible setting. Their distributions in the position-velocity space are shown in Fig. 1B. The driving optical forces significantly shift the distributions away from the undriven ones. Black curves in Fig. 1B are measured trajectories evolving from a given point to a different point in the position-velocity space during forward (or reverse) processes. Due to thermal fluctuation, it is not possible to have two trajectories starting from exactly the same point in the phase space. Here we use (x, v) to represent points within $(x \pm \frac{\sigma_x}{11}, v \pm \frac{\sigma_v}{11})$, where σ_x and σ_v are the standard deviations of the position and velocity distributions, respectively.

Fig. 2 shows our experimental results of testing DFT with a 209-nm-radius nanosphere in the underdamped regime (see supplemental online material for more information). The optical force (Fig. 2A) is monitored using a fraction of the 532-nm laser split from the main beam. Fig. 2B-C show the dynamic evolution of the nanosphere in the position and velocity coordinates, respectively. Since the irreversible ramps ($\sim 4.6 \mu\text{s}$) are faster than the velocity ($\sim 8.6 \mu\text{s}$) and position ($\sim 100 \mu\text{s}$) relaxation times, the nanosphere is far from thermal equilibrium when the ramps finish.

With the acquired position, velocity and force data, the DFT is ready to be tested. The DFT in Eq. 1 can be rewritten in the position coordinate as, $\frac{P_R(-W, x_2 \rightarrow x_1)}{P_F(W, x_1 \rightarrow x_2)} = \frac{P_R(x_2 \rightarrow x_1)}{P_F(x_1 \rightarrow x_2)} \frac{P_R(-W|x_2 \rightarrow x_1)}{P_F(W|x_1 \rightarrow x_2)}$ [20]. Here $P_F(x_1 \rightarrow x_2)$ is the probability of having a forward trajectory going from x_1 to x_2 ,

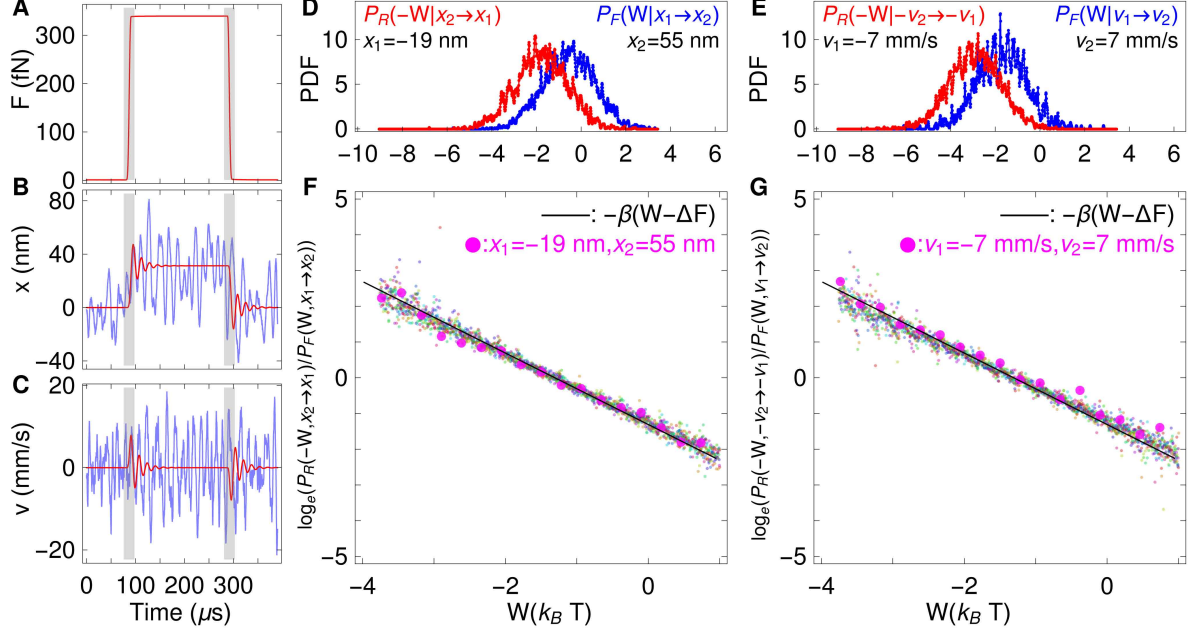


FIG. 2. Testing the differential fluctuation theorem in the underdamped regime. **A**, Optical force. **B-C**, Measured position and velocity trajectories. A single trajectory is shown in blue, and the averaged trajectory of over one million trajectories is shown in red. The gray shaded regions in **A-C** denote the forward and reverse intervals, respectively. It takes roughly $4.6 \mu\text{s}$ for the optical force strength to switch from 10% to 90% level. **D**, An example of probabilities $P_F(W|x_1 \rightarrow x_2)$ and $P_R(-W|x_2 \rightarrow x_1)$ in position coordinate. **E**, An example of probabilities $P_F(W|v_1 \rightarrow v_2)$ and $P_R(-W|-v_2 \rightarrow -v_1)$ in velocity coordinate. **F, G** Testing the DFT in position and velocity spaces. The small markers with different colors represent measurements of $\log_e \frac{P_R(-W, x_2 \rightarrow x_1)}{P_F(W, x_1 \rightarrow x_2)}$ and $\log_e \frac{P_R(-W, -v_2 \rightarrow -v_1)}{P_F(W, v_1 \rightarrow v_2)}$ for 121 different $\{x_1, x_2\}$ and $\{v_1, v_2\}$ combinations, respectively. The big magenta markers are results for parameters shown in **D** and **E**, respectively. The black lines represent $-\beta(W - \Delta F)$.

and $P_R(x_2 \rightarrow x_1)$ is the probability of a reverse trajectory going from x_2 to x_1 . These quantities can be calculated using the distributions illustrated in the Fig. 1B. They are essentially equivalent to the number of forward (reverse) trajectories going from x_1 to x_2 (x_2 to x_1). $P_F(W|x_1 \rightarrow x_2)$ is the probability of performing work W for those forward trajectories going from x_1 to x_2 , and $P_R(-W|x_2 \rightarrow x_1)$ is the reverse probability (Fig. 2D). Similarly, Fig. 2E shows examples of $P_F(W|v_1 \rightarrow v_2)$ and $P_R(-W|-v_2 \rightarrow -v_1)$ in the velocity coordinate. The minus sign ($-$) in the velocity space is due to the time reversal symmetry of the reverse

process. Here irreversible work is calculated as $W = -\sum_{i=1}^{n-1}(f_{i+1} - f_i)(x_i + x_{i+1})/2$ for n successive position and force measurements. This formula is obtained using the Hamiltonian, $H = \frac{1}{2}kx^2 - fx + \frac{1}{2}mv^2$, and the work definition $W = \int_0^\tau dt \dot{f}(t) \frac{\partial H}{\partial f}$ during a ramp period τ [2]. Here k is the trap stiffness.

The DFT is tested in detail using 121 different initial-final combinations in the position and velocity coordinates uniformly distributed in $(\pm\sigma_x, \pm\sigma_v)$. Fig. 2F shows that the left hand side, $\frac{P_R(-W, x_2 \rightarrow x_1)}{P_F(W, x_1 \rightarrow x_2)}$, agrees well with the right hand side, $e^{-\beta(W-\Delta F)}$, of the DFT in Eq. 1. Here $e^{-\beta(W-\Delta F)}$ is a function of the work variable W . The free energy difference can be calculated as $\Delta F = -(f_{\text{on}}^2 - f_{\text{off}}^2)/(2k) = -1.3 k_B T$ with $f_{\text{off}}/f_{\text{on}} = 0/340$ fN (Fig. 2A). Similarly, we can verify the DFT in the velocity coordinate (Fig. 2G). Data points also distribute closely to the curves $e^{-\beta(W-\Delta F)}$. Thus our data agree with the DFT well in position and velocity coordinates simultaneously.

Our experimental data can also test other fluctuation theorems which are direct integrations of the DFT. Integrating the Eq. 1 over W and b , we obtain the generalized JE in the position and velocity coordinates ($a = x$ or $a = v$) [19, 24, 27],

$$\begin{aligned}\langle e^{-\beta(W-\Delta F)} | x_i = x \rangle_F &= P_R(x_f = x) / P_F(x_i = x), \\ \langle e^{-\beta(W-\Delta F)} | v_i = v \rangle_F &= P_R(v_f = -v) / P_F(v_i = v).\end{aligned}\tag{2}$$

Here $P_F(x_i = x)$ is the probability that a forward trajectory *initializes* at x , and $P_R(x_f = x)$ is the probability that a reverse trajectory *finalizes* at x . Similarly, $P_F(v_i = v)$ and $P_R(v_f = -v)$ are the probabilities in the velocity coordinate. They are essentially equivalent to the number of trajectories *initialized* (*finalized*) at x or v . The value $\langle e^{-\beta(W-\Delta F)} | x_i = x \text{ (or } v_i = v) \rangle_F$ is averaged over all forward trajectories initialized at x or v in the position or velocity coordinates. The data agree well with the generalized JE as shown in Fig. 3A,B. For slow ramps, the measured $\langle e^{-\beta(W-\Delta F)} | x_i \text{ (or } v_i) \rangle_F$ stays closely to 1, which is the result of a reversible process. However, for fast (irreversible) ramps, the values of $\langle e^{-\beta(W-\Delta F)} | x_i \text{ (or } v_i) \rangle_F$ diverge away from 1, so the generalized JE is needed to explain our observations.

Similarly, integrating Eq. 1 over W and a leads to the HSR in the position and velocity spaces ($b = x$ or $b = v$) [6, 19, 20],

$$\begin{aligned}\langle e^{-\beta(W-\Delta F)} | x_f = x \rangle_F &= P_R(x_i = x) / P_F(x_f = x), \\ \langle e^{-\beta(W-\Delta F)} | v_f = v \rangle_F &= P_R(v_i = -v) / P_F(v_f = v).\end{aligned}\tag{3}$$

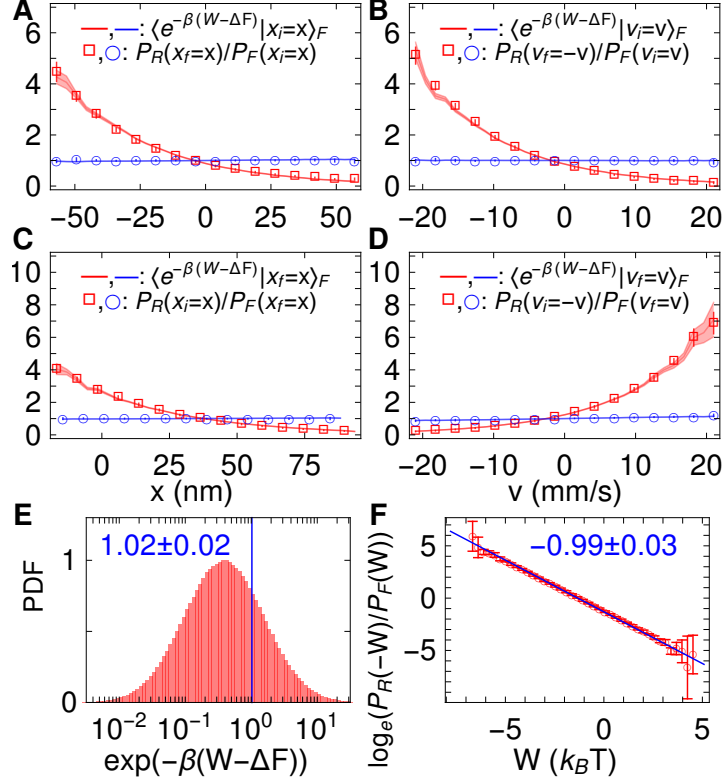


FIG. 3. Testing fluctuation theorems in the underdamped regime. **A**, **B**, Testing generalized JE in position and velocity spaces for a fast ramp (red, $4.6 \mu\text{s}$ from 10% to 90% levels), and a slow ramp (blue, $40 \mu\text{s}$ from 10% to 90% levels). Markers represent the measured $P_R(x_f = x)/P_F(x_i = x)$ and $P_R(v_f = -v)/P_F(v_i = v)$ in position and velocity spaces, respectively. **C**, **D**, Testing HSR in position and velocity spaces for a fast ramp (red) and a slow ramp (blue). Markers represent the measured $P_R(x_i = x)/P_F(x_f = x)$ and $P_R(v_i = -v)/P_F(v_f = v)$ in position and velocity spaces, respectively. The errorbars of $P_R(x)/P_F(x)$ and $P_R(-v)/P_F(v)$ represent the standard deviation of the measurements for 20 equal divisions in each subset x and v , respectively. The markers represent their mean values. In **A–D**, the shaded line represent $\langle e^{-\beta(W-\Delta F)} \rangle$, where its thickness represents the uncertainty of 600 work (Joule) calibrations. **E**, Testing the JE using forward irreversible work, $\langle e^{-\beta(W-\Delta F)} \rangle = 1.02 \pm 0.02$ (vertical line). **F**, Testing the CFT. The slope of the linear fit yields a value -0.99 ± 0.03 . In **E–F**, The errorbars and the uncertainty are due to the standard deviation of 600 work (Joule) calibrations.

Here $\langle e^{-\beta(W-\Delta F)} | x_f = x \text{ (or } v_f = v) \rangle_F$, $P_F(x_f = x)$, and $P_R(x_i = x)$ are denoted using the same conventions as in the generalized JE in Eq. 2. The data agree well with the HSR for

both fast (irreversible) ramps and slow (reversible) ramps as shown in Fig. 3C,D.

The JE [2] can be obtained by integrating Eq. 1 over a , b and W . The data show an excellent agreement with JE, $\langle e^{-\beta(W-\Delta F)} \rangle = 1.02 \pm 0.02$ (Fig. 3E). The CFT [4] can be obtained by integrating Eq. 1 over a and b , $P_R(-W)/P_F(W) = e^{-\beta(W-\Delta F)}$. The measurements of $\log_e(P_R(-W)/P_F(W))$ show an excellent agreement with a linear fit (Fig. 3F). The fit yields a linear slope of -0.99 ± 0.03 which agrees well with the theoretical slope of -1 .

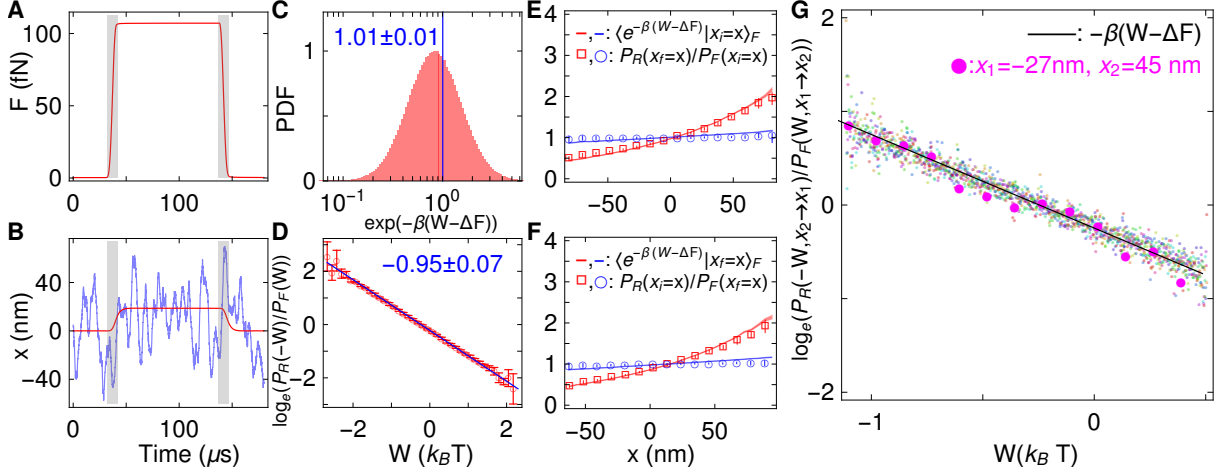


FIG. 4. Testing DFT and FT in the overdamped regime. **A**, The optical force. **B**, The average of over 1 million position trajectories is shown in red, and a single trajectory is shown in blue. **C**, Testing the JE using the forward irreversible work, $\langle e^{-\beta(W-\Delta F)} \rangle = 1.01 \pm 0.01$ (vertical line). **D**, Testing the CFT. The slope of the linear fit yields -0.95 ± 0.07 . In **C–D**, The errorbars and the uncertainty are the standard deviation of 600 work (Joule) calibrations. **E**, Testing the generalized JE in position space for a fast ramp (red, $4.8 \mu\text{s}$ from 10% to 90% level), and a slow ramp (blue, $62 \mu\text{s}$ from 10% to 90% level). **F**, Testing the HSR in position space for a fast ramp, and a slow ramp. In **E–F**, the shaded line represent $\langle e^{-\beta(W-\Delta F)} \rangle$, where its thickness represents the uncertainty due to 600 work (Joule) calibrations. The errorbars of $P_R(x_i = x)/P_F(x_f = x)$ represent the standard deviation of the measurements for 20 equal divisions within the range between $x - \frac{\sigma_x}{11}$ and $x + \frac{\sigma_x}{11}$. The markers represent their mean values. **G** Testing differential fluctuation theorem in position space. The small markers with different colors represent the measurements of $\log_e \frac{P_R(-W, x_2 \rightarrow x_1)}{P_F(W, x_1 \rightarrow x_2)}$ for 121 different combinations $\{x_1, x_2\}$. The large magenta markers illustrate data for the combination $\{-27 \text{ nm}, 45 \text{ nm}\}$. The black line represents $-\beta(W - \Delta F)$.

For completeness, we also tested the DFT in the overdamped regime ($a = x_1$ and $b = x_2$)

where the velocity relaxes to equilibrium much faster than other processes. So it is sufficient to measure the position only. The optical force profile and the position trajectories are shown in Fig. 4A,B. For a typical optical force, $f_{\text{off}}/f_{\text{on}} = 0/107$ fN, the free energy difference is $\Delta F = -0.24 k_B T$. As shown in Fig. 4B, the nanosphere position is far from the equilibrium when the ramps finish. The experimental data show good agreements with the JE [2], the CFT [4], the generalized JE [24], HSR [6], and the DFT [20] as shown in Fig. 4C–G.

Overall, the differential fluctuation theorem unifies many existing fluctuation theorems [9, 10, 18, 24, 27, 28, 31], such as JE, CFT, HSR, EFR, and FTLB, and is arguably the most detailed fluctuation theorem that can be tested experimentally. The DFT can also improve free energy calculations [20]. Our experimental results validate the DFT [20] well in both underdamped and overdamped regimes. Our work deepens our understanding of the second law to an unprecedentedly detailed level. It initiates the experimental study of stochastic thermodynamics with instantaneous velocity measurements, and may shed new light on our understanding of the origin of time’s arrow [33].

-
- [1] Jarzynski, C. Equalities and inequalities: Irreversibility and the second law of thermodynamics at the nanoscale. *Annu. Rev. Condens. Matter Phys.* **2**, 329 (2011).
 - [2] Jarzynski, C. Nonequilibrium equality for free energy differences. *Phys. Rev. Lett.* **78**(14), 2690 (1997).
 - [3] Liphardt, J., Dumont, S., Smith, S. B., Tinoco, I., and Bustamante, C. Equilibrium information from nonequilibrium measurements in an experimental test of Jarzynski’s equality. *Science* **296**, 1832–1835 (2002).
 - [4] Crooks, G. E. Entropy production fluctuation theorem and the nonequilibrium work relation for free energy differences. *Phys. Rev. E* **60**(3), 2721 (1999).
 - [5] Collin, D., Ritort, F., Jarzynski, C., Smith, S. B., Tinoco, I., and Bustamante, C. Verification of the Crooks fluctuation theorem and recovery of RNA folding free energies. *Nature* **437**(7056), 231–234 (2005).
 - [6] Hummer, G. and Szabo, A. Free energy reconstruction from nonequilibrium single-molecule pulling experiments. *Proc. Natl. Acad. Sci.* **98**(7), 3658–3661 (2001).
 - [7] Harris, N. C., Song, Y., and Kiang, C.-H. Experimental free energy surface reconstruction

- from single-molecule force spectroscopy using Jarzynski's equality. *Phys. Rev. Lett.* **99**, 068101 (2007).
- [8] Gupta, A. N., Vincent, A., Neupane, K., Yu, H., Wang, F., and Woodside, M. T. Experimental validation of free-energy-landscape reconstruction from non-equilibrium single-molecule force spectroscopy measurements. *Nature Phys.* **7**(8), 631–634 (2011).
 - [9] Junier, I., Mossa, A., Manosas, M., and Ritort, F. Recovery of free energy branches in single molecule experiments. *Phys. Rev. Lett.* **102**(7), 070602 (2009).
 - [10] Alemany, A., Mossa, A., Junier, I., and Ritort, F. Experimental free-energy measurements of kinetic molecular states using fluctuation theorems. *Nature Phys.* **8**(9), 688–694 (2012).
 - [11] Wang, G., Sevick, E. M., Mittag, E., Searles, D. J., and Evans, D. J. Experimental demonstration of violations of the second law of thermodynamics for small systems and short time scales. *Phys. Rev. Lett.* **89**(5), 050601 (2002).
 - [12] Trepagnier, E., Jarzynski, C., Ritort, F., Crooks, G. E., Bustamante, C., and Liphardt, J. Experimental test of Hatano and Sasa's nonequilibrium steady-state equality. *Proc. Natl. Acad. Sci.* **101**(42), 15038–15041 (2004).
 - [13] Douarche, F., Joubaud, S., Garnier, N. B., Petrosyan, A., and Ciliberto, S. Work fluctuation theorems for harmonic oscillators. *Phys. Rev. Lett.* **97**, 140603 (2006).
 - [14] Jun, Y., Gavrilov, M., and Bechhoefer, J. High-precision test of Landauer's principle in a feedback trap. *Phys. Rev. Lett.* **113**, 190601 (2014).
 - [15] Gieseler, J., Quidant, R., Dellago, C., and Novotny, L. Dynamic relaxation of a levitated nanoparticle from a non-equilibrium steady state. *Nat. Nanotechnol.* **9**(5), 358–364 (2014).
 - [16] Lee, D. Y., Kwon, C., and Pak, H. K. Nonequilibrium fluctuations for a single-particle analog of gas in a soft wall. *Phys. Rev. Lett.* **114**(6), 060603 (2015).
 - [17] Pekola, J. P. Towards quantum thermodynamics in electronic circuits. *Nature Phys.* **11**, 118 (2015).
 - [18] Seifert, U. Entropy production along a stochastic trajectory and an integral fluctuation theorem. *Phys. Rev. Lett.* **95**(4), 040602 (2005).
 - [19] Kawai, R., Parrondo, J. M. R., and den Broeck, C. V. Dissipation: the phase space perspective. *Phys. Rev. Lett.* **98**, 080602 (2007).
 - [20] Maragakis, P., Spichty, M., and Karplus, M. A differential fluctuation theorem. *J. Phys. Chem. B* **112**(19), 6168–6174 (2008).

- [21] Esposito, M. and den Broeck, C. V. Three detailed fluctuation theorems. *Phys. Rev. Lett.* **104**, 090601 (2010).
- [22] Sagawa, T. and Ueda, M. Generalized Jarzynski equality under nonequilibrium feedback control. *Phys. Rev. Lett.* **104**(9), 090602 (2010).
- [23] Toyabe, S., Sagawa, T., Ueda, M., Muneyuki, E., and Sano, M. Experimental demonstration of information-to-energy conversion and validation of the generalized Jarzynski equality. *Nature Phys.* **6**(12), 988–992 (2010).
- [24] Gong, Z. and Quan, H. Jarzynski equality, Crooks fluctuation theorem, and the fluctuation theorems of heat for arbitrary initial states. *Phys. Rev. E* **92**(1), 012131 (2015).
- [25] Blickle, V., Speck, T., Helden, L., Seifert, U., and Bechinger, C. Thermodynamics of a colloidal particle in a time-dependent nonharmonic potential. *Phys. Rev. Lett.* **96**, 070603 (2006).
- [26] Martinez, I. A., Roldan, E., Dinis, L., Petrov, D., Parrondo, J. M. R., and Rica, R. A. Brownian Carnot engine. *Nature Phys.* **12**, 67 (2016).
- [27] Crooks, G. E. *Excursions in Statistical Dynamics*. PhD Thesis. University of California, Berkeley, (1999).
- [28] den Broeck, C. V. Stochastic thermodynamics: A brief introduction. *Proceedings of the International School of Physics Enrico Fermi* **184**, 155 (2013).
- [29] Jarzynski, C. Hamiltonian derivation of a detailed fluctuation theorem. *J. Stat. Phys.* **98**(1-2), 77–102 (2000).
- [30] Li, T., Kheifets, S., Medellin, D., and Raizen, M. G. Measurement of the instantaneous velocity of a Brownian particle. *Science* **328**(5986), 1673–1675 (2010).
- [31] Camunas-Soler, J., Alemany, A., and Ritort, F. Experimental measurement of binding energy, selectivity, and allostery using fluctuation theorems. *Science* **355**, 412–415 (2017).
- [32] Hoang, T. M., Ahn, J., Bang, J., and Li, T. Electron spin control of optically levitated nanodiamonds in vacuum. *Nat. Commun.* **7**, 12250 (2016).
- [33] Feng, E. H. and Crooks, G. E. Length of time’s arrow. *Phys. Rev. Lett.* **101**, 090602 (2008).

METHODS

Calibrations in underdamped regime. The force data shown in Fig. 2A indicate that forward and reverse forces have good time-reversal symmetry with only $\sim 1\%$ difference in the area under the force curve. The particle velocity shown in Fig. 2C is calculated after binning 7 position points together to reduce the detection noise [30]. The nanosphere velocity has a signal-to-noise ratio of about 8.9. Here the particle position-velocity (x - v) is calibrated to SI units using the equipartition theorem, $k\langle x^2 \rangle = k_B T$. $k = (4/3)\pi r^3 \rho \Omega^2$ is the trap stiffness. The silica nanosphere has a mass density of $\rho = 1960 \text{ kg/m}^3$ (Bangs Laboratories). The power spectra and position autocorrelation function [32] yield a hydrodynamic radius $r = 209 \pm 9 \text{ nm}$ and a trapping frequency $\Omega/2\pi = 60.4 \pm 0.3 \text{ kHz}$. The optical force is calibrated using Hooke's law, $f = k\Delta x$, with Δx being the position displacement. The work (Joule) calibration is the product of the position and force calibrations.

Parameters for testing DFT and FT in overdamped regime. A smaller nanosphere with a hydrodynamic radius $r = 145 \pm 5 \text{ nm}$ is used for testing DFT and FT in overdamped regime. It is levitated at a pressure of 760 torr. The trapping frequency is $\Omega = 76 \pm 3 (2\pi \cdot \text{kHz})$. These parameters are extracted from 600 position samples ($\sim 50 \text{ ms/sample}$). Over one million experimental forward-reverse cycles are performed.

DATA AVAILABILITY

The data that support the findings of this study are available from the corresponding authors upon reasonable request.

AUTHOR CONTRIBUTIONS

T.L., H.T.Q., T.M.H., and R.P. conceived and designed the project. T.M.H., J.A, J.B. built the experimental apparatus. T.M.H. performed measurements. T.M.H. and R.P. analyzed the data. T.L. and H.T.Q. supervised the work. All authors co-wrote the paper.

COMPETING FINANCIAL INTERESTS

The authors declare no competing financial interests.